Integrated Ionic Liquid and Rate-Based Absorption Process Design for Carbon Capture: Global Optimization Using Hybrid Models

Xiang Zhang[1], Xuechong Ding[2], Zhen Song[2], Teng Zhou[1,2,*], Kai Sundmacher[1,2]

[1] Process Systems Engineering, Max Planck Institute for Dynamics of Complex Technical Systems, Sandtorstr. 1, D-39106 Magdeburg, Germany

[2] Process Systems Engineering, Otto-von-Guericke University Magdeburg, Universitätsplatz 2, D-39106 Magdeburg, Germany

[*] Corresponding author: zhout@mpi-magdeburg.mpg.de (Teng Zhou)

First submission: December 2020

Abstract

A new method for integrated ionic liquid (IL) and absorption process design is proposed where a rigorous rate-based process model is used to incorporate absorption thermodynamics and kinetics. Different types of models including group contribution models and thermodynamic models are employed to predict the process-relevant physical, kinetic, and thermodynamic (gas solubility) properties of ILs. Combining the property models with process models, the integrated IL and process design problem is formulated as an MINLP optimization problem. Unfortunately, due to the model complexity, the problem is prone to convergence failure. To lower the computational difficulty, tractable surrogate models are used to replace the complex thermodynamic models while maintaining the prediction accuracy. This provides an opportunity to find the global optimum for the integrated design problem. A pre-combustion carbon capture case study is provided to demonstrate the applicability of the method. The obtained global optimum saves 14.8% cost compared to the Selexol process.

Keywords: computer-aided ionic liquid design, rate-based absorption, hybrid modelling, carbon capture, global optimization

1. Introduction

CO_2 mitigation is crucial for protecting the global climate and environment. Carbon capture and storage (CCS) is a promising route to reduce CO_2 emissions. For CCS, carbon capture is a key procedure where CO_2 should be economically separated from various types of flue gases.[1] Among the existing carbon capture technologies, solvent-based absorption is the most mature one. For instance, the dimethyl ether of polyethylene glycol (DEPG) has been used in the Selexol process for pre-combustion carbon capture although this technology still suffers from some drawbacks such as low mass transfer rate and high energy consumption. Since the core for employing absorption processes lies in the use of high-performing solvents, the search for new advanced solvents is essential for enhancing the carbon capture performance.[2]

Ionic liquids (ILs) are potential solvents for carbon capture due to their high CO_2 solubility, low volatility as well as chemical and thermal stability.[3,4] However, the number of ILs is almost infinite when considering the large number of anions, cations, and substituent groups. Clearly, using the traditional trial-and-error method is inefficient for selecting optimal ILs.[5] So far, many efforts have been made on computational IL screening. Various predictive models and tools such as *ab initio* methods, equations of state (EOS), activity coefficient models have been utilized to estimate the thermodynamic properties of ILs for IL screening. For instance, Jing et al.[5] used the density function theory (DFT) method to calculate specific performance indicators on CO_2 absorption to screen multi-amino-functionalized ILs. It is noted that *ab initio* methods are computationally expensive and barely applied with large databases although they can offer useful insights on some thermodynamic properties. For screening ILs with large CO_2 solubility at moderate pressures, the COSMO-RS and COSMO-SAC models have been extensively applied to predict the activity coefficient and subsequently the CO_2-in-IL solubilities.[6-9] At a high pressure, these models can be combined with an EOS such as Peng-Robinson (PR).[10] Although these approaches can efficiently screen ILs with desired properties, they are limited by the number of available IL candidates in the databases. To further expand the search space and find new ILs, a systematic approach for IL design is highly necessary.

For organic solvent design, computer-aided molecular design (CAMD) methods have been developed and successfully applied.[11-14] The solvent is represented as a set of descriptors (e.g., functional groups or topological descriptors) and its properties are calculated using property

prediction models. The solvent design problem is then formulated as an optimization problem where certain solvent properties are maximized or minimized to generate optimal solvent molecular structures. By following this strategy, computer-aided IL design (CAILD) approaches have been proposed.[15-18] Similarly, the IL is decomposed into different structural groups. Based on quantitative structure-property relationship (QSPR) models, IL structure is optimized to achieve desired properties.[19] For predicting IL physical properties (e.g., melting point and viscosity), simple linear group contribution (GC) models are suitable and can be easily applied.[20-22] Besides, for predicting thermodynamic properties (e.g., activity coefficient and solubility) of IL systems, the nonlinear GC-based UNIFAC models are often used.[23,24] In order to make accurate predictions, the involved UNIFAC model parameters for IL systems have been extensively fitted from experimental data.[25,26]

It is worth noting that any solvent ultimately serves a specific process and the process performance depends on the solvent selection and process operations.[27,28] Given the strong interdependency between these two issues, integrated IL and process design is always preferred for enhancing the overall process efficiency.[29,30] In the literature, the simultaneous design of ILs and processes has been studied for separating azeotropic mixtures.[31-33] For carbon capture, Valencia-Marquez et al.[16] proposed an optimization approach for integrated IL and absorption process design. To reduce the computational difficulty, a short-cut absorption process model was employed and only the absorption thermodynamics is considered. Recently, the key role of absorption kinetics over thermodynamics in IL selection for CO_2 capture has been revealed.[34-36] Ignoring kinetics can lead to sub-optimal or even poor solutions. To identify truly optimal ILs for CO_2 capture, a rigorous rate-based absorption process model that incorporates both absorption thermodynamics and kinetics should be used. In this work, a new computer-aided IL and process design (CAILPD) method is developed for carbon capture based on the rigorous rate-based absorption process model where the effects of ILs on absorption thermodynamics and kinetics are simultaneously considered.

Moreover, integrated IL and process design problems are usually formulated as complex mixed-integer nonlinear programming (MINLP) problems. Such optimization problems are intractable to global optimality, especially when strong nonlinear property models and rigorous process models are used.[27,37] Recently, surrogate models that are constructed based on reliable data have been widely used in process optimization to substitute complicated thermodynamic or process models.[38,39] This can effectively lower the computational difficulty while maintaining the model reliability. Thus, it motivates us to incorporate the surrogate

modeling technique into the proposed CAILPD framework for achieving a convergence to global optimality that usually cannot be obtained otherwise. The paper is organized as follows. First, the CAILPD framework is introduced. Afterwards, the CAILPD approach is applied and demonstrated on a pre-combustion carbon capture case study.

2. CAILPD Framework

Figure 1 shows the framework for computer-aided ionic liquid and rate-based absorption process design. The design problem can be decomposed into two main steps, a forward prediction or simulation step (blue solid lines) and a reverse design or optimization step (red dash lines). The forward step relates IL molecular structure and process operating conditions with the final process performance via different types of models. As illustrated, the effects of ILs on the mass transfer coefficient of absorption are quantified by employing QSPR or group contribution (GC) models and certain correlation equations. On the other hand, gas fugacity and activity coefficients in the vapor and liquid phases can be predicted by traditional thermodynamic models and the equilibrium gas solubility is then calculated through the solution of the vapor-liquid equilibrium (VLE) equation. Alternatively, the thermodynamic equilibrium solubility can be directly predicted by surrogate models. Substituting the mass transfer coefficient and thermodynamic driving force into the rate-based absorption model, the corresponding process performance can thus be evaluated for a given IL and process condition. After completing the forward step, the best IL structure and optimal process conditions can be reversely identified by solving an MINLP problem where the process performance is optimized considering all the models or equations as well as IL structural constraints.

[Insert Figure 1 here]

3. CAILPD for Pre-combustion Carbon Capture

3.1 Representation of ILs

The first step for designing ILs is to decompose them into different building blocks. ILs can be represented in different ways. In this work, an IL is decomposed into an anion, a cation core, and substituents linked to the cation core. This representation can provide large design space and flexibility.[33] Taking 1-propyl-3-methylimidazolium

bis(trifluoromethylsulfonyl)imide [C_3mim][Tf_2N] as an example (see Figure 2), this IL is constituted by an anion 'Tf_2N', a cation core 'Im13', and 4 substituent groups including 1 'aN_CH_3', 1 'aN_CH_2', 1 'CH_2', and 1 'CH_3'.

[Insert Figure 2 here]

In the present work, 23 anions, 12 cation cores, and 17 cation substituent groups are considered for the IL design, as listed in Table 1(a). Each generated IL is denoted by a vector $n=[n_1,\ldots,n_i,\ldots,n_N]$ where N = 52 and the element n_i represents the number of the i-th building group presented in the IL molecule. Note that only the abbreviations of groups are given and their molecular structures are shown in Table S1 (Supporting Information). In addition, their contributions to properties (e.g., molecular weight, melting point, etc.) and the upper bounds in the CAILPD program are listed in Table S1 as well. These contributions are considered as parameters in the following sections. Note that the nomenclature is presented at the end of the Supporting Information.

[Insert Table 1 here]

3.2 IL structural constraints

To generate a feasible IL, certain structural constraints must be satisfied. A feasible IL consists of only one anion and one cation (Eq. 1-2). Eq. 3 shows that the number of each constituent group should be non-negative and less than its upper bound n_i^{upp}. The total number of constituent groups including cation, anion, and substituent groups is between 2 and 8.

$$\sum_{i\in G_{anion}} n_i = 1 \tag{1}$$

$$\sum_{i\in G_{cation}} n_i = 1 \tag{2}$$

$$0 \le n_i \le n_i^{upp} \qquad \forall i \in G_{tot} \tag{3}$$

$$2 \le \sum_{i\in G_{tot}} n_i \le 8 \qquad G_{tot} = [G_{cation}, G_{anion}, G_{i}] \tag{4}$$

The octet rule in Eq. 5 ensures that an IL has zero valency. $PV\,A_i$ is the valency of the i-th constituent group. The modified bonding rule in Eq. 6 ensures that two adjacent groups in an IL are not linked by more than one bond.

$$\sum_{i\in G_{cation}\cup G_{i}} n_i \cdot (2 - PV\,A_i) = 2 \tag{5}$$

$$n_i \cdot (PV\ A_i - 1) + 2 \leq \sum_{j \in G_{cation} \cup G_{i}} n_j \qquad \forall i \in \{G_{cation}, G_{i}\} \tag{6}$$

Eq. 7 means that the total number of functional substituent groups is no more than that of the alkyl substituent groups. G_{fg} and G_{ag} are the sets of functional and alkyl substituent groups, respectively. The detailed classification of cation substituent groups are given in Table 1 (b).

$$\sum_{i \in G_{fg}} n_i \leq \sum_{j \in G_{ag}} n_j \tag{7}$$

Eq. 8-9 ensure that the total number of ether and hydroxyl groups (G_{eh}) is less than 2 and less than the total number of non-CH_3 alkyl groups (G_{nCH_3}), respectively. In addition, the total number of fluorized alkyl groups (G_{fag}) is less than 2 (Eq. 10). Ether and hydroxyl groups and fluorized alkyl groups cannot exist simultaneously (Eq. 11).

$$\sum_{i \in G_{eh}} n_i \leq 2 \tag{8}$$

$$\sum_{i \in G_{eh}} n_i \leq \sum_{j \in G_{nCH_3}} n_j \tag{9}$$

$$\sum_{i \in G_{fag}} n_i \leq 2 \tag{10}$$

$$\sum_{i \in G_{eh}} n_i \cdot \sum_{j \in G_{fag}} n_j = 0 \tag{11}$$

Eq. 12-16 ensure that the cation is properly linked to the corresponding substituent groups. G_{aN} and G_{cycN} are the sets of alkyl groups linked to the aromatic and cyclic nitrogen, respectively. G_N and G_P are the alkyl groups linked to acyclic nitrogen and acyclic phosphorous, respectively.

$$\left(\frac{n_{\Im 13}}{2} + n_{MIm} + n_{MMIM} + n_{Py} + n_{MPy}\right) \cdot \sum_{i \in G_{aN}} n_i + \left(n_{MPyrro} + n_{MPip}\right) \cdot \sum_{i \in G_{cycN}} n_i + \left(\frac{n_N}{4} + \frac{n_{NH}}{3} + \frac{n_{NH_2}}{2} + n_{NH_3}\right) \cdot \sum_{i \in G_N} n_i + \frac{n_P}{4} \cdot \sum_{i \in G_P} n_i \tag{12}$$

$$\left(n_{\Im 13} + n_{MIm} + n_{MMIM} + n_{Py} + n_{MPy}\right) \cdot \left(\sum_{i \in G_{cycN}} n_i + \sum_{i \in G_N} n_i + \sum_{i \in G_P} n_i\right) = 0 \tag{13}$$

$$\left(n_{MPyrro} + n_{MPip}\right) \cdot \left(\sum_{i \in G_{aN}} n_i + \sum_{i \in G_N} n_i + \sum_{i \in G_P} n_i\right) = 0 \tag{14}$$

$$\left(n_N + n_{NH} + n_{NH_2} + n_{NH_3}\right) \cdot \left(\sum_{i \in G_{cycN}} n_i + \sum_{i \in G_{aN}} n_i + \sum_{i \in G_P} n_i\right) = 0 \tag{15}$$

$$n_P \cdot \left(\sum_{i \in G_{cycN}} n_i + \sum_{i \in G_{aN}} n_i + \sum_{i \in G_N} n_i \right) = 0 \quad (16)$$

Eq. 17-20 ensure that if the cation is only linked to CH_3, no other substituent groups can exist. G_{DCH_3} and G_{NDC} are the sets of CH_3 group directly linked to cation and group not directly linked to cation, respectively.

$$(n¿¿MIm + n_{MMIM} + n_{Py} + n_{MPy} + n_{MPyrro} + n_{MPip} + n_{NH_3}) \cdot (0 - \sum_{i \in G_{DCH_3}} n_i) \cdot \sum_{j \in G_{NDC}} n_j \geq 0¿ \quad (17)$$

$$(n¿¿\Im 13 + n_{NH_2}) \cdot (1 - \sum_{i \in G_{DCH_3}} n_i) \cdot \sum_{j \in G_{NDC}} n_j \geq 0¿ \quad (18)$$

$$n_{NH} \cdot (2 - \sum_{i \in G_{DCH_3}} n_i) \cdot \sum_{j \in G_{NDC}} n_j \geq 0 \quad (19)$$

$$(n¿¿N + n_P) \cdot (3 - \sum_{i \in G_{DCH_3}} n_i) \cdot \sum_{j \in G_{NDC}} n_j \geq 0¿ \quad (20)$$

3.3 IL physical and kinetic property prediction

Physical and kinetic properties of ILs are required for the rate-based process modelling. Figure 3 summarizes different models for predicting the physical and kinetic properties of ILs. The detailed model descriptions are elaborated below.

[Insert Figure 3 here]

3.3.1 GC models to physical properties

The molecular weight (MW), melting point (T_m), boiling point (T_b), critical temperature (T_c), and critical pressure (P_c) of ILs are calculated using the GC methods in Eq. 21-25.[40,41] PMW_i, PTm_i, PTb_i, PTc_i, and PPc_i are the contributions of the i-th group to the corresponding properties (see Table S1).

$$MW = \sum_{i \in G_{tot}} n_i \cdot PMW_i \quad (21)$$

$$T_m = 288.7 + \sum_{i \in G_{tot}} n_i \cdot PTm_i \quad (22)$$

$$T_b = 198.2 + \sum_{i \in G_{tot}} n_i \cdot PTb_i \quad (23)$$

$$T_c = \frac{T_b}{0.5703 + 1.0121 \sum_{i \in G_{tot}} n_i \cdot PTc_i - \left(\sum_{i \in G_{tot}} n_i \cdot PTc_i \right)^2} \quad (24)$$

$$P_c = \frac{MW}{\left(0.34 + \sum_{i \in G_{tot}} n_i \cdot PPc_i \right)^2} \quad (25)$$

IL molar volume (MV) depends on the temperature (T) and pressure (P) in Eq. 26. The molar volume (MV_0) at $T_0 = 298.15\,K$ and $P_0 = 1.0$ ¿ is calculated using the GC approach in Eq. 27. PMV_i is the i-th group's contribution to molar volume (see Table S1).[42]

$$MV = MV_0 \cdot \left[1 + \frac{6.439 (T - T_0)}{10000} \right] \cdot \left[1 - 0.081 \times \ln \left(1 + \frac{(1 + 0.00497 (T - T_0))(P - P_0)}{1950} \right) \right] \quad (26)$$

$$MV_0 = \sum_{i \in G_{tot}} n_i \cdot PMV_i \quad (27)$$

An artificial neural network (ANN) based GC model has been developed to predict IL viscosity.[43] The model consists of three layers (i.e., input layer, hidden layer, and output layer). Based on the ANN-GC model, the viscosity (μ) of ILs is estimated by

$$sn_x = \frac{2 \sum_{i \in G_{tot}} b^0_{x,i} \cdot n_i}{w^0_x} - 1 \qquad x = 1, \ldots, 242 \quad (28)$$

$$vis_y = \sum_{x=1}^{242} sn_x \cdot w^1_{y,x} + \frac{(2T - 826.15) w^1_{y,T}}{319.85} + \frac{(2P - 3500.6) w^1_{y,P}}{3499.4} + b^1_y \qquad y = 1, \ldots, 7 \quad (29)$$

$$f^{one}(vis_y) = 1 - \frac{2}{1 + e^{2 \times vis_y}} \quad (30)$$

$$f^{two} = \sum_{y=1}^{7} w^2_y \cdot f^{one}(vis_y) \quad (31)$$

$$\mu = 7.87\, e^{6.33995 f^{two} - 6.11685} \quad (32)$$

where w^0_x and $b^0_{x,i}$ are the normalization factors. $w^1_{y,x}$, $w^1_{y,T}$, and $w^1_{y,P}$ are the weighting factors in the hidden layer. b^1_y is the bias in the hidden layer. w^2_y is the weighting factor in the output layer. These parameters can be found in Ref. [43].

3.3.2 Correlation models to physical and kinetic properties

The density (ρ), thermal conductivity (λ), and heat capacity (C_p) of ILs are calculated using the following correlation functions.[41,44]

$$\rho = \frac{1000 \times MW}{MV} \tag{33}$$

$$\lambda = \left[\frac{11.1}{T^{1.091}} + \frac{0.6107}{0.1369\, MW^{0.5817}} \left(\frac{T_b}{T_c} \right)^{0.552} \right] \cdot \left[1 - 0.007 \left(\frac{P}{P_c} \right)^{0.7} \right] \tag{34}$$

$$C_p = \frac{7.7 + 0.226\left(T - 298.15\right) + 1.918\, MV}{MW} \tag{35}$$

Moreover, when ILs are used for CO_2 absorption in a packed column, it can be assumed that mass transfer resistance occurs in the vicinity of gas-liquid interface. With this, the mass transfer coefficient (k) can be estimated using the Onda' correlation.[45,46]

$$k \left(\frac{\rho}{1000 \times \mu \cdot g} \right)^{\frac{1}{3}} = 0.000051 \times Re_w^{\frac{2}{3}} \cdot \left(a_p \cdot d_p \right)^{0.4} \cdot Sc^{-0.5} \tag{36}$$

where g is the gravity constant. a_p and d_p are the specific packing surface area and diameter, respectively. *Sc* is the Schmidt number calculated in Eq. 37. The mass diffusivity coefficient D_{mass} is obtained using the modified Wilke–Chang correlation[47] where ϕ is the association factor and MV^{CO_2} is the molar volume of CO_2 solute at its boiling point.[48] Packing provides a low pressure drop and high efficiency for gas absorption thus it is used in this work.[49]

$$Sc = \frac{\mu}{10^3 \times \rho \cdot D_{mass}} \tag{37}$$

$$D_{mass} = 7.4 \times 10^{-12} \frac{\phi^{0.5} \cdot MW^{0.67} \cdot T}{\mu^{0.58} \cdot \left(MV^{CO_2} \right)^{0.6}} \tag{38}$$

In addition, Re_w is the Reynolds number depending on the wet interfacial area a_w.

$$Re_w = \frac{M^{IL} \cdot MW}{CSA \cdot \mu \cdot a_w} \tag{39}$$

$$a_w = a_p \left[1 - e^{-1.45 \sigma_{cp}^{0.75} \cdot \sigma^{-0.75} \cdot Re^{0.1} \cdot Fr^{-0.05} \cdot We^{0.2}} \right] \tag{40}$$

where M^{IL} is the molar flowrate of ILs and *CSA* is the cross-section area of absorption column. σ_{cp} is the critical surface tension of packings. σ is the surface tension of ILs. The

dimensionless Reynolds number $\Re$, Froude number Fr, and Weber number We are calculated by

$$\Re = \frac{M^{IL} \cdot MW}{CSA \cdot \mu \cdot a_p} \tag{41}$$

$$Fr = \left(\frac{M^{IL} \cdot MW}{10^3 \rho} \right)^2 \cdot \frac{a_p}{CSA^2 \cdot g} \tag{42}$$

$$We = \frac{\left(M^{IL} \cdot MW \right)^2}{10^6 \times CSA^2 \cdot \rho \cdot \sigma \cdot a_p} \tag{43}$$

3.4 CO_2 solubility in ILs

3.4.1 Rigorous thermodynamic model

Based on thermodynamics, the vapor-liquid equilibrium (VLE) of CO_2 determines its solubility in ILs. At equilibrium, the molar fraction of CO_2 in ILs ($x_{CO_2}^{eq}$) can be expressed as

$$x_{CO_2}^{eq} = \frac{\varphi_{CO_2} \cdot y_{CO_2} \cdot P}{\gamma_{CO_2} \cdot Psat_{CO_2}} \tag{44}$$

$$Psat_{CO_2} = 10 \times e^{\left(12.3312 - \frac{4759.46}{T + 156.462} \right)} \tag{45}$$

where y_{CO_2} is the molar fraction of CO_2 in the gas phase. $Psat_{CO_2}$ is the saturated pressure of CO_2 (in bar), estimated by the extrapolated Antoine equation in Eq. 45. The fugacity coefficient φ_{CO_2} can be predicted using the Peng-Robinson (PR) model and the activity coefficient γ_{CO_2} can be calculated by the UNIFAC model.[24] The detailed description of the PR and UNIFAC models is presented in Appendix A.

3.4.2 ANN-based solubility model

Alternatively, the CO_2 equilibrium solubility in ILs can be predicted by surrogate models. By using ANN and support vector machine algorithms, Song et al.[50] recently built two GC-based machine learning models to predict CO_2 equilibrium solubility in ILs. These two models were developed from a comprehensive database containing more than 10,000 CO_2 solubility data in various ILs at different temperatures and pressures. The mean absolute error and R^2 of the two models are less than 0.03 and larger than 0.97, respectively. These statistics indicate that the models can give reliable predictions on CO_2 equilibrium solubility.

Moreover, according to the reported model errors, the ANN model is slightly better and thus is applied here. The ANN-GC model consists of a three-layer feed forward network. The input layer receives IL structure information and temperature and pressure. The hidden layer comprising of 7 neurons transfers the input to the output layer where the CO_2 solubility is finally predicted. Specifically, the CO_2 equilibrium molar fraction $x_{CO_2}^{eq}$ is calculated by the following equations.

$$NN_t^1 = \sum_i NW_{t,i}^1 \cdot n_i + TW_t^1 \cdot T + PW_t^1 \cdot P \cdot y_{CO_2} + bW_t^1 \qquad t = 1, \ldots, 7 \tag{46}$$

$$NN_t^2 = 1 - \frac{2}{1 + e^{2 \times NN_t^1}} \tag{47}$$

$$x_{CO_2}^{eq} = \sum_{t=1}^{7} NW_t^2 \cdot NN_t^2 + bW^2 \tag{48}$$

where the superscripts 1 and 2 denote the hidden layer and output layer, respectively. Subscripts *t* and *i* are the neuron and IL group indices, respectively. NW, TW, and PW are weighting factors to IL group numbers, temperature, and pressure, respectively. bW represents the bias. All these parameters can be found in Ref.[50]

3.5 IL-based absorption process model

Figure 4 illustrates the schematic diagram of IL-based absorption process for CO_2 capture. The feed gas is first compressed and cooled (if necessary) since high pressure and low temperature are favored for dissolving CO_2. Then, the compressed gas is fed to an absorber where it counter-currently contacts with the ILs. Meanwhile, CO_2 goes into the IL phase while other gases remain in the gas phase. The CO_2-rich ILs leave from the bottom of the absorber while the clean gas is collected from the top. Afterwards, the CO_2-loaded ILs are heated and enter a flash tank which has a lower pressure than the absorber. In the flash tank, the captured CO_2 is released and collected. Later, the recovered ILs are cooled and sent back to the absorber. In addition, makeup ILs are added to the absorber in case of IL losses. The specific process models used for CAILPD are presented below.

[Insert Figure 4 here]

3.5.1 Compressor

The feed gas is compressed to match the pressure in the absorber (P^{AB}). Assuming an adiabatic compression, the compressor workload W^{COMP} in kW and the output temperature T_{out}^{COMP} are calculated by Eq. 49 and Eq. 50, respectively.

$$W^{COMP}=\frac{1}{1000}\times\frac{IC}{IC-1}\cdot M^{feed}\cdot MV^{feed}\cdot P^{feed}\cdot\left[\left(\frac{P^{AB}}{P^{feed}}\right)^{\frac{IC-1}{IC}}-1\right] \tag{49}$$

$$T_{out}^{COMP}=T^{feed}\cdot\left(\frac{P^{AB}}{P^{feed}}\right)^{\frac{IC-1}{IC}} \tag{50}$$

where M^{feed}, MV^{feed}, P^{feed}, and T^{feed} are the molar flowrate, molar volume, pressure, and temperature of the feed gas, respectively. IC is the isentropic coefficient.

3.5.2 Heat exchanger for gas cooling

The compressed feed gas is cooled to match the temperature in the absorber (T^{AB}). Assuming that the heat exchanger has a counter-current design, the logarithm mean temperature difference $LMTD^{GC}$ is calculated as

$$LMTD^{GC}=\frac{\left(T_{out}^{COMP}-T_{out}^{water}\right)-\left(T^{AB}-T_{¿}^{water}\right)}{\ln\left(T_{out}^{COMP}-T_{out}^{water}\right)-\ln\left(T^{AB}-T_{¿}^{water}\right)} \tag{51}$$

where $T_{¿}^{water}$ and T_{out}^{water} are the inlet and outlet temperature of cooling water, respectively. In addition, the removed heat (Q^{GC} in kJ/s), heat transfer area (HTA^{GC}), and mass flowrate of cooling water (mw^{GC}) are calculated from the energy balances.

$$Q^{GC}=Cp^{feed}M^{feed}MV^{feed}\rho^{feed}\left(T_{out}^{COMP}-T^{AB}\right) \tag{52}$$

$$Q^{GC}=1000\times Cp^{water}mw^{GC}\left(T_{out}^{water}-T_{¿}^{water}\right)=\frac{HTA^{GC}\cdot LMTD^{GC}\cdot U^{GC}}{1000} \tag{53}$$

whereCp^{feed} and ρ^{feed} are the heat capacity and density of the feed gas, respectively. U^{GC} is the overall heat transfer coefficient (200 W/(m^2·K)) in the gas-cooling heat exchanger.

3.5.3 Absorber

The rate-based model is used in the absorber. The column is presumably isothermal and T^{AB} should be larger than the melting temperature to ensure that the ILs are in liquid. In addition, the column is divided into $NT=20$ sections. In each section, the amount of CO_2 absorbed from gas to ILs ($pern$) is equal and decided from the mass balance.

$$T_m \le T^{AB} \tag{54}$$

$$pern = \frac{M^{feed} \cdot y_{CO_2}^{feed} \cdot \theta}{NT} \tag{55}$$

where $y_{CO_2}^{feed}$ and θ are the CO_2 molar fraction in the feed gas and the percentage of CO_2 to be absorbed, respectively. If the solubility of other gases in ILs is negligible, the liquid and vapor molar fractions of CO_2 in the n-th section ($n = 1, \ldots, NT$ from the bottom up) can be calculated by

$$x_{n,CO_2} = \frac{M^{IL} x_{out,CO_2}^{FT} + (NT - n)\, pern}{M^{IL} + (NT - n)\, pern} \tag{56}$$

$$y_{n,CO_2} = \frac{M^{feed} y_{CO_2}^{feed} - n \times pern}{M^{feed} - n \times pern} \tag{57}$$

where x_{out,CO_2}^{FT} is the molar fraction of CO_2 in the ILs regenerated from the flash tank (FT). In addition, the following summation equations must be satisfied for each section.

$$\sum_c x_{n,c} = 1 \tag{58}$$

$$\sum_c y_{n,c} = 1 \tag{59}$$

where the subscript c denotes the gas and liquid components. Moreover, the height of the n-th section (h_n) is calculated in Eq. 60 and the height of the absorber H^{AB} is obtained by Eq. 61.[46]

$$pern \cdot \frac{MV^{IL}}{10^6} = Void_p \cdot a_w \cdot CSA \cdot k \cdot h_n \cdot \left(\frac{x_{n,CO_2}^{eq}}{1 - x_{n,CO_2}^{eq}} - \frac{x_{n,CO_2}}{1 - x_{n,CO_2}} \right) \tag{60}$$

$$H^{AB} = \sum_{n=1}^{NT} h_n \tag{61}$$

where MV^{IL} denotes the molar volume of IL in the absorber (see Eq. 26-27). $Void_p$ is the void fraction of packing. x_{n,CO_2}^{eq} represents the equilibrium CO_2 solubility in the n-th column section. If rigorous thermodynamic models are used, it is calculated using Eq. 44-45 with known y_{n,CO_2}. Alternatively, this equilibrium solubility can be directly calculated by Eq. 46-48 if the ANN-based surrogate model is applied. In addition, Eq. 62 ensures a positive driving force for CO_2 absorption.

$$x_{n,CO_2}^{eq} \geq x_{n,CO_2} \tag{62}$$

3.5.4 Heat exchanger for IL heating

The CO_2-rich ILs are heated by steam in a shell-and-tube heat exchanger. The IL and steam flow through the shell and tube, respectively. Wadekar[51] reported that the average heat transfer coefficient for this type of heat exchanger U^{HE} is about 946 W/(m^2·K). The $LMTD^{HE}$ is written as

$$LMTD^{HE} = \frac{\left(T^{steam} - T^{AB}\right) - \left(T^{steam} - T^{FT}\right)}{\ln\left(T^{steam} - T^{AB}\right) - \ln\left(T^{steam} - T^{FT}\right)} \tag{63}$$

where T^{steam} and T^{FT} are the steam temperature and the temperature of the flash tank, respectively. In addition, the required heat duty (Q^{HE} in kJ/s) is calculated by

$$Q^{HE} = \frac{Cp^{HE} \cdot M^{IL} \cdot MW \cdot \left(T^{FT} - T^{AB}\right)}{1000} \tag{64}$$

where the IL heat capacity Cp^{HE} is predicted by Eq. 35 at an average temperature ($\frac{T^{FT} + T^{AB}}{2}$). The mass flowrate of the consumed steam (ms^{HE} in kg/s) and the heat transfer area (HTA^{HE}) are calculated below. LH is the latent heat of steam.

$$Q^{HE} = ms^{HE} \cdot LH = \frac{HTA^{HE} \cdot U^{HE} \cdot LMTD^{HE}}{1000} \tag{65}$$

3.5.5 Flash tank

The heated CO_2-loaded ILs are fed into the flash tank for solvent regeneration. The temperature in the flash tank cannot exceed the boiling point of IL to prevent its vaporization. The CO_2 molar fraction in the lean ILs x_{out,CO_2}^{FT} is estimated by the short-cut model in Eq. 67.[52]

$$T^{FT} < T_b \tag{66}$$

$$x_{out,CO_2}^{FT} = 1 - \frac{1}{1 + \frac{P^{FT} \cdot MW}{10^4 \exp\left(6.8591 - \frac{2004.3}{T^{FT}}\right)}} \tag{67}$$

In order to facilitate the computation in the absorber, x_{out,CO_2}^{FT} is fixed to 0.02. In this case, the operating pressure of the flash tank P^{FT} depends on the temperature T^{FT}. Moreover, the flash tank is presumably operated on a half-full basis and the total volume of ILs in the flash tank is equal to the volume of 5 minutes' IL flows.[53] Thus, the volume of the flash tank (V^{FT}) is expressed as

$$V^{FT}=2\times 300\times M^{IL}\cdot\frac{MV^{FT}}{10^{6}} \tag{68}$$

where MV^{FT} is the IL molar volume at T^{FT} and P^{FT}.

3.5.6 Pump

The regenerated ILs are pumped back to the absorber. The pump workload W^{PUMP} in kW is estimated by

$$W^{PUMP}=10^{-4}\cdot M^{IL}\cdot MV^{FT}\cdot\left(P^{AB}-P^{FT}\right) \tag{69}$$

3.5.7 Heat exchanger for IL cooling

Similarly, a shell-and-tube heat exchanger is used for IL cooling. The heat transfer coefficient U^{CO} is assumed to be 946 W/(m^2·K) according to Ref.[51] The $LMTD^{CO}$, the removed heat Q^{CO} in kJ/s, the mass flowrate of cooling water mw^{CO} in ton/s, and heat transfer area HTA^{CO} are calculated below.

$$LMTD^{CO}=\frac{\left(T^{FT}-T_{out}^{water}\right)-\left(T^{AB}-T_{¿}^{water}\right)}{\ln\left(T^{FT}-T_{out}^{water}\right)-\ln\left(T^{AB}-T_{¿}^{water}\right)} \tag{70}$$

$$Q^{CO}=\frac{Cp^{CO}\cdot M^{IL}\cdot MW\cdot\left(T^{FT}-T^{AB}\right)}{1000} \tag{71}$$

$$Q^{CO}=10^{3}\times Cp^{water}\,mw^{CO}\left(T_{out}^{water}-T_{¿}^{water}\right)=\frac{HTA^{CO}\cdot U^{CO}\cdot LMTD^{CO}}{1000} \tag{72}$$

3.5.8 Process economics

The performance of the IL-based carbon capture process is evaluated using the total annualized cost (*TAC*).

$$TAC=CRF\cdot C_{cap}+C_{ope} \tag{73}$$

$$C_{cap}=C^{COMP}+C^{GC}+C^{HE}+C^{CO}+C^{PUMP}+C^{AB}+C^{FT} \tag{74}$$

$$C_{ope} = C^{steam} + C^{ele} + C^{water} + C^{ml} \quad (75)$$

where CRF is the capital recovery factor. C_{cap} is the summation of the capital costs of all the equipment. C_{ope} is the annual operating cost that accounts for the consumption of utilities (i.e., steam, electricity, and cooling water) and other operating costs including labor, maintenance, and IL losses. The detailed calculation of the capital and operating costs is presented in Appendix B.

4. Results and Discussion

As a major CO_2 emission resource, the pre-combustion flue gas is usually produced in an integrated gasification combined cycle (IGCC) based power plant. The feedstock such as natural gas is reacted with oxygen under high temperature and pressure to produce synthesis gas consisting of CO, H_2, and CO_2. Through a water-gas shift reaction, the CO is converted into CO_2 and the pre-combustion flue gas comprising mainly H_2 and CO_2 is formed. The CO_2 must be removed from the H_2 before power generation. In this work, the CAILPD framework is applied for pre-combustion carbon capture. The flue gas is assumed to be at 313.15 K and 20 bar with a molar flowrate of 10 kmol/s. The compositions of CO_2 and H_2 are set to 0.4 and 0.6, respectively. With an assumption that H_2 is not soluble in the ILs, the goal is to design a cost-effective IL-based absorption process for capturing no less than 90% CO_2 from the flue gas.

4.1 First trail using rigorous thermodynamic model

In the first trial, the CAILPD problem is formulated using the classic thermodynamic models (i.e., UNIFAC and PR models) to predict the CO_2 equilibrium solubility. An MINLP problem is formed and summarized below. The objective is to minimize the process TAC while fulfilling the carbon capture requirement stated above. The design variables (degrees of freedom) consist of the discrete variable n_i and the continuous variables P^{AB} and T^{FT}. Equality constraints include IL structural constraints, property and process models as well as process economics. The specific feed gas conditions as well as process and costing parameters are listed in Table 2. The UNIFAC model parameters for the CO_2-IL systems can be found in Zhou et al.[26]

$$\min_{n_i, P^{AB}, T^{FT}} TAC$$

s.t.	Eq. 1−20	IL structural constraints
	Eq. 21−45, A1−A14	IL property models
	Eq. 54−62	Absorption model
	Eq. 49−53, 63−72	Other process models
	Eq. 73−75, B1−B15	Process economics

[Insert Table 2 here]

The optimization problem is coded in GAMS 24.2 and solved using the deterministic global optimization solver BARON version 19.3.24.[54] The computational statistics are listed in the second column of Table 3. As shown, in total 52 discrete variables, 3086 single variables, 3121 equations, and 58032 nonlinear matrix entries are involved. Clearly, this is a very complicated optimization problem. Different initial estimates and different ways of formulating equations are considered. However, it cannot converge within 24 hours on a standard computer.

[Insert Table 3 here]

4.2 Second trail using ANN-based solubility model

In order to mitigate the computational difficulties, the highly complex thermodynamic models are replaced by the relatively simple ANN-based surrogate model. Furthermore, Eq. 76 serves as an upper bound that limits the CO_2 equilibrium solubility at a specific absorption condition lower than 0.5. This absorption condition corresponds to the case where the feed gas is cooled and directly fed into the absorber. This constraint ensures that the ANN model does not extrapolate to unreasonable predictions.

$$x_i^{eq} = F\left(n_i, T = T^{AB}, P = 20, y_{CO2} = 0.4\right) \le 0.5 \quad (76)$$

F_{ANN} represents Eq. 46–48. Replacing Eq. 44–45 and Eq. A1−A14 in the previous MINLP problem with Eq. 46–48 and adding Eq. 76 as an extra constraint, we can formulate another MINLP problem. The new optimization problem is solved with the global solver BARON as well. The third column of Table 3 lists the corresponding computational statistics. It consists of 52 discrete variables, 439 single variables, 456 equations, and 574 nonlinear matrix entries. It is clear that the problem size and nonlinearity are much less than those of the previous problem. It takes around 1.5 hours for BARON to converge to the global optimality.

The obtained optimal IL and its properties as well as the operating conditions and process specifications are summarized in Table 4. The corresponding minimized process *TAC* is 11.44 M$/year. The optimal IL found is N-ethyl-N-ethoxymethyl-ammonium bis(pentafluoroethanesulfonyl)amide [EEOMA][BETA] or N-ethyl-N-methoxyethyl-ammonium bis(pentafluoroethanesulfonyl)amide [EMOEA][BETA] that consists of the anion BETA, the cation core NH_2, and 5 substituent groups (2 N_CH_2, 2 CH_3, and 1 OCH_2). The operating pressure in the absorber is 21.5 bar and the temperature in the flash tank is 334.9 K. The averaged CO_2 equilibrium solubility (molar fraction) in the absorber is as high as 0.458. In addition, the IL viscosity in the absorber is 10.3 mPa·s. Comparing with most of the known ILs,[43] this value is quite small, resulting in a high CO_2 mass transfer coefficient.

[Insert Table 4 here]

The DEPG-based Selexol process is widely used for pre-combustion carbon capture. As a benchmark, the economic performance of the Selexol process is evaluated. The flowsheet of the Selexol process is shown in Figure S1 (Supporting Information). It is simulated in Aspen Plus V8.8 according to literature reports[55,56] and the detailed process specifications are listed in Table S2. For consistency, the process economics is assessed with the same cost models used in this work. Figure 5 compares the cost breakdown of the two processes. As indicated, although a much larger amount of steam and cooling water are consumed in the IL-based process, the electricity cost of the Selexol process is much higher than that of the IL-based process. This is because a higher pressure (30 bar) is needed in the absorber of the Selexol process to meet the CO_2 capture requirement, which leads to a larger electricity consumption for gas compressing. In contrast, our designed IL has a higher CO_2 solubility than DEPG, making the absorption operable at a lower pressure (21.5 bar). In total, the IL-based process can achieve 14.8% total cost reduction compared to the benchmark Selexol process for pre-combustion carbon capture, which demonstrates the significance and large benefit of integrated IL and process design.

[Insert Figure 5 here]

5. Conclusion

This paper presents a new integrated IL and absorption process design approach for carbon capture. The physical, kinetic, and thermodynamic properties of ILs are predicted by different types of methods (e.g., GC methods, empirical correlations, rigorous thermodynamic and

data-driven models). In order to improve the reliability of the results, a rigorous rate-based absorption model, where both absorption thermodynamics and kinetics are incorporated, is used. With these, the integrated IL and process design task is formulated and solved as an MINLP optimization problem. The IL structure and process operating conditions are simultaneously optimized to minimize the total annualized cost. The proposed approach is demonstrated on a pre-combustion carbon capture example. In the case study, rigorous thermodynamic models (UNIFAC and PR) are first applied to predict the CO_2 equilibrium solubility in ILs, which results in a convergence failure of the MINLP problem. To tackle the problem, an ANN-based surrogate model is used to replace the thermodynamic models. Based on this, the integrated design problem is successfully solved to the global optimality. The result shows that compared to the DEPG-based Selexol process, the optimal IL-based process can achieve a better economic performance for the investigated carbon capture task.

To the best of our knowledge, this work is the first attempt in the global optimization of an integrated IL and process design problem where rigorous rate-based process model is employed. This study can be extended in several ways. For instance, the method can be applied to handle different CO_2 emission sources. In addition, the IL-based absorption process can be compared with other carbon capture processes (e.g., adsorption and membrane) to identify the most efficient technology for different carbon sources. Despite the large progress, limitations should not be neglected. First, a simple inequality constraint is added to prevent unreasonable extrapolation of the ANN-based solubility model. In the future work, more advanced methods (e.g., convex hull[57] and topological data analysis[58]) can be used to confine the results into the validity region. Second, the current work cannot distinguish between structural isomers. To do so, higher-order GC models incorporating the group connectivity information are required, which may significantly increase the computational demand. A more realistic strategy is to investigate the practical performance of isomers in a post-design step, for example, by experimental studies. Efforts in these directions are underway.

Acknowledgments

The authors acknowledge the financial support from Max Planck Society, Germany to the Ernst Dieter Gilles Postdoctoral Fellowship for Xiang Zhang and to the Computer-Aided Material and Process Design (CAMPD) project.

Appendix A

UNIFAC activity coefficient model

The activity coefficient of CO_2 in ILs is calculated by the reformulated UNIFAC model.[59] The combinatorial part γ_s^C and residual part γ_s^R are given in Eq. A2 and Eq. A3 – A7, respectively.

$$\ln \gamma_s = \ln\left(\gamma_s^C\right) + \ln\left(\gamma_s^R\right) \tag{A1}$$

$$\ln\left(\gamma_s^C\right) = \ln\left(R_s\right) - \ln \text{¿} \tag{A2}$$

$$\ln\left(\gamma_s^R\right) = R1_s - R2_s \tag{A3}$$

$$R1_s = Q_s - \sum_i n_{s,i} \cdot q_i \cdot \ln\left(R3_i\right) + Q_s \ln\left(\sum_{ss} x_{ss} Q_{ss}\right) - \sum_i \frac{R4_{s,i}}{R3_i} \tag{A4}$$

$$R2_s = Q_s \ln\left(Q_s\right) - \sum_i n_{s,i} \cdot q_i \cdot \ln\left(\sum_{ii} q_{ii} n_{s,ii} \psi_{ii,i}\right) \tag{A5}$$

$$R3_i = \sum_{ii} q_{ii} \sum_{ss} n_{ss,ii} x_{ss} \psi_{ii,i} \tag{A6}$$

$$R4_{s,i} = \sum_{ii} n_{s,ii} q_{ii} q_i \sum_{ss} n_{ss,i} x_{ss} \psi_{ii,i} \tag{A7}$$

where the subscripts *s* and *ss* are component indexes. *i* and *ii* are group indexes. *x* and *n* represent the component molar fraction and number of group, respectively. The molecular Van der Waals volume and surface area as well as the group interaction parameter are determined by Eq. A8 – A10.

$$R_s = \sum_i n_{s,i} r_i \tag{A8}$$

$$Q_s = \sum_i n_{s,i} q_i \tag{A9}$$

$$\psi_{ii,i} = e^{\frac{-a_{ii,i}}{T}} \tag{A10}$$

The group volume and surface area r_i and q_i as well as the binary group interaction parameter $a_{ii,i}$ for the CO_2-IL systems can be found in Zhou et al.[26]

Peng-Robinson fugacity model

The fugacity of CO_2 is calculated using the PR model.

$$\ln \phi_{CO_2} = B B_{CO_2}(Z-1) - \ln(¿ Z - B) - \frac{A}{2\sqrt{2}B}(A A_{CO_2} - B B_{CO_2}) \ln\left(\frac{Z+(1+\sqrt{2})B}{Z+(1-\sqrt{2})B}\right) ¿ \quad \text{(A11)}$$

$$Z^3 - (1-B)Z^2 + (A - 3B^2 - 2B)Z - (AB - B^2 - B^3) = 0 \quad \text{(A12)}$$

The intermediate variables are calculated by

$$A A_{CO_2} = \frac{2}{a_{\sum ¿}[\sum_j^{n_c}(y_j \cdot a a_{j,CO_2})]¿}, \quad A = \frac{a_{\sum ¿} \cdot P}{R^2 T^2} ¿, \quad a_{\sum ¿} = \sum_j^{n_c}\sum_{jj}^{n_c}(y_j \cdot y_{jj} \cdot a a_{j,jj}) ¿,$$

$$a a_{j,jj} = a a_{jj,j} = (1 - \delta_{j,jj}) a a_j^{0.5} a a_{jj}^{0.5}, \quad a a_j = 0.45724 \frac{\alpha_j \cdot R^2 T c_j^2}{P c_j},$$

$$\alpha_j = \left[1 + \left(1 - \sqrt{\frac{T}{Tc}}\right) \cdot (0.37464 + 1.54226\,\omega_j - 0.26992\,\omega_j^2)\right]^2 \quad \text{(A13)}$$

$$B B_{CO_2} = \frac{b b_{CO_2}}{b_{\sum ¿} ¿}, \quad B = \frac{b_{\sum ¿} \cdot P}{RT} ¿, \quad b_{\sum ¿} = \sum_i^{n_c} y_j b b_j ¿, \quad b b_j = 0.0778 \frac{R \cdot T c_j}{P c_j} \quad \text{(A14)}$$

where Z is the compressibility factor. R and T are the ideal gas constant and gas temperature, respectively. T_c, P_c, and ω are the critical temperature, critical pressure, and acentric factor, respectively. The subscripts j and jj represent the gas components. n_c is the total number of components.aa_j and bb_j are pure-component parameters. $a_{\sum ¿ ¿}$ and $b_{\sum ¿ ¿}$ are mixture parameters. $\delta_{j,jj}$ is the binary interaction parameter between components j and jj (δ_{CO_2,H_2}= −0.1622).

Appendix B

Capital cost

Comparing with reference cases, the capital cost of compressor (C^{COMP}), heat exchangers (C^{GC}, C^{HE}, and C^{CO}), and pump (C^{PUMP}) depends on the workload, heat transfer area, and volumetric flowrate, respectively.[53]

$$C^{COMP} = C_{ref}^{COMP} \cdot \frac{W^{COMP}}{W_{ref}^{COMP}} \quad \text{(B1)}$$

$$C^{GC}=C_{ref}^{HEX}\cdot\frac{A^{GC}}{A_{ref}^{HEX}},\quad C^{HE}=C_{ref}^{HEX}\cdot\frac{A^{HE}}{A_{ref}^{HEX}},\quad C^{CO}=C_{ref}^{HEX}\cdot\frac{A^{CO}}{A_{ref}^{HEX}} \tag{B2}$$

$$C^{PUMP}=C_{ref}^{PUMP}\cdot\frac{M^{IL}\cdot MV^{FT}}{VF_{ref}^{PUMP}} \tag{B3}$$

where C_{ref}^{COMP}, C_{ref}^{HEX}, and C_{ref}^{PUMP} are the reference cost of compressor, heat exchanger, and pump, respectively. W_{ref}^{COMP} is the reference compressor workload, A_{ref}^{HEX} is the reference heat exchanger area, and VF_{ref}^{PUMP} is the reference volumetric flowrate. Furthermore, the capital cost of absorber (C^{AB}) consists of the costs of column shell (C_{cs}), packing (C_{pa}), and platform and ladder (C_{pl}) where C_{cs} depends on the weight of the column shell W^{AB} in Eq. B6.[53]

$$C^{AB}=1.218\left(C_{cs}+C_{pa}+C_{pl}\right) \tag{B4}$$

$$C_{cs}=2.0706\,e^{6.629+0.1826\ln W^{AB}+0.02297\left(\ln W^{AB}\right)^2} \tag{B5}$$

$$W^{AB}=\rho^{steel}\left[H^{AB}\frac{\pi\left(D^{AB}+2\Omega^{AB}\right)^2-\pi\left(D^{AB}\right)^2}{4}+2\cdot\frac{\pi\left(D^{AB}\right)^2}{4}\cdot\Omega^{AB}\right] \tag{B6}$$

$$C_{pa}=2681\times CSA\cdot H^{AB} \tag{B7}$$

$$C_{pl}=300\left(D^{AB}\right)^{0.7396}\cdot\left(H^{AB}\right)^{0.7068} \tag{B8}$$

where ρ^{steel} is the density of steel. D^{AB} and Ω^{AB} are the inner diameter and thickness of the absorber, respectively. The capital cost of flash tank C^{FT} is decided by its weight W^{FT}.[53]

$$C^{FT}=3.5112\,e^{8.571-0.233\ln W^{FT}+0.04333\left(\ln W^{FT}\right)^2}+2291\left(3.28\,D^{FT}\right)^{0.2029} \tag{B9}$$

$$W^{FT}=\rho^{steel}\cdot¿ \tag{B10}$$

where D^{FT} and Ω^{FT} are the inner diameter and thickness of the flash tank, respectively.

Operating cost

Since steam is used to heat the CO_2-loaded IL up, the steam cost C^{steam} depends on the mass flowrate of steam consumed in the heat exchanger (ms^{HE}). The electricity cost C^{ele} accounts for the electricity consumption in the compressor (W^{COMP}) and pump (W^{PUMP}). In addition, the cost of cooling water C^{water} covers the water consumption for IL and feed gas cooling. Moreover, it is assumed that one process cycle takes 1000 seconds and 0.01‰ of the total ILs used in one cycle is lost every day. Thus, the cost of IL losses is calculated in Eq.

B14. Finally, the labor and maintenance cost is assumed to be 16 percent of the total capital cost.

$$C^{steam} = 330 \times 24 \times 3600 \times ms^{HE} \cdot PR^{steam} \quad \text{(B11)}$$

$$C^{ele} = 330 \times 24 \times \left(W^{COMP} + W^{PUMP}\right) \cdot PR^{ele} \quad \text{(B12)}$$

$$C^{water} = 330 \times 24 \times 3600 \times \left(mw^{CO} + mw^{GC}\right) \cdot PR^{water} \quad \text{(B13)}$$

$$C^{IL} = 330 \times 10^{-5} \times 1000 \cdot M^{IL} \cdot MW \cdot PR^{IL} \quad \text{(B14)}$$

$$C^{ml} = 0.16 \cdot C_{cap} + C^{IL} \quad \text{(B15)}$$

where PR^{steam}, PR^{ele}, PR^{water} and PR^{IL} are the prices of steam, electricity, cooling water, and ionic liquid, respectively.

Literature cited

1. Zaman M, Lee JH. Carbon capture from stationary power generation sources: a review of the current status of the technologies. *Korean J Chem Eng.* 2013;30(8):1497-1526.
2. Papadopoulos AI, Badr S, Chremos A, et al. Computer-aided molecular design and selection of CO_2 capture solvents based on thermodynamics, reactivity and sustainability. *Mol Syst Des Eng.* 2016;1(3):313-334.
3. Ramdin M, de Loos TW, Vlugt TJH. State-of-the-art of CO_2 capture with ionic liquids. *Ind Eng Chem Res.* 2012;51(24):8149-8177.
4. Zhang X, Zhang X, Dong H, Zhao Z, Zhang S, Huang Y. Carbon capture with ionic liquids: overview and progress. *Energy Environ Sci.* 2012;5(5):6668-6681.
5. Wang J, Song Z, Cheng H, Chen L, Deng L, Qi Z. Computer-aided design of ionic liquids as absorbent for gas separation exemplified by CO_2 capture cases. *ACS Sustain Chem Eng.* 2018;6(9):12025-12035.
6. Zhang X, Liu Z, Wang W. Screening of ionic liquids to capture CO_2 by COSMO-RS and experiments. *AIChE J.* 2008;54(10):2717-2728.
7. Song Z, Zhou T, Zhang J, Cheng H, Chen L, Qi Z. Screening of ionic liquids for solvent-sensitive extraction –with deep desulfurization as an example. *Chem Eng Sci.* 2015;129:69-77.
8. Lee B-S, Lin S-T. Screening of ionic liquids for CO_2 capture using the COSMO-SAC model. *Chem Eng Sci.* 2015;121:157-168.

9. Zhao Y, Gani R, Afzal RM, Zhang X, Zhang S. Ionic liquids for absorption and separation of gases: an extensive database and a systematic screening method. *AIChE J.* 2017;63(4):1353-1367.

10. Mortazavi-Manesh S, Satyro MA, Marriott RA. Screening ionic liquids as candidates for separation of acid gases: solubility of hydrogen sulfide, methane, and ethane. *AIChE J.* 2013;59(8):2993-3005.

11. Wang Y, Achenie LEK. Computer aided solvent design for extractive fermentation. *Fluid Phase Equilib.* 2002;201(1):1-18.

12. Karunanithi AT, Achenie LEK, Gani R. A new decomposition-based computer-aided molecular/mixture design methodology for the design of optimal solvents and solvent mixtures. *Ind Eng Chem Res.* 2005;44(13):4785-4797.

13. Karunanithi AT, Achenie LEK, Gani R. A computer-aided molecular design framework for crystallization solvent design. *Chem Eng Sci.* 2006;61(4):1247-1260.

14. Austin ND, Sahinidis NV, Trahan DW. Computer-aided molecular design: an introduction and review of tools, applications, and solution techniques. *Chem Eng Res Des.* 2016;116:2-26.

15. Chávez-Islas LM, Vasquez-Medrano R, Flores-Tlacuahuac A. Optimal molecular design of ionic liquids for high-purity bioethanol production. *Ind Eng Chem Res.* 2011;50(9):5153-5168.

16. Valencia-Marquez D, Flores-Tlacuahuac A, Vasquez-Medrano R. An optimization approach for CO_2 capture using ionic liquids. *J Clean Prod.* 2017;168:1652-1667.

17. Chen Y, Koumaditi E, Gani R, Kontogeorgis GM, Woodley JM. Computer-aided design of ionic liquids for hybrid process schemes. *Comput Chem Eng.* 2019;130:106556.

18. Liu X, Chen Y, Zeng S, et al. Structure optimization of tailored ionic liquids and process simulation for shale gas separation. *AIChE J.* 2020;66(2):e16794.

19. Karunanithi AT, Mehrkesh A. Computer-aided design of tailor-made ionic liquids. *AIChE J.* 2013;59(12):4627-4640.

20. Chong FK, Foo DCY, Eljack FT, Atilhan M, Chemmangattuvalappil NG. Ionic liquid design for enhanced carbon dioxide capture by computer-aided molecular design approach. *Clean Technol Environ Policy.* 2015;17(5):1301-1312.

21. Chong FK, Eljack FT, Atilhan M, Foo DCY, Chemmangattuvalappil NG. A systematic visual methodology to design ionic liquids and ionic liquid mixtures: green solvent alternative for carbon capture. *Comput Chem Eng.* 2016;91:219-232.

22. Song Z, Zhang C, Qi Z, Zhou T, Sundmacher K. Computer-aided design of ionic liquids as solvents for extractive desulfurization. *AIChE J.* 2018;64(3):1013-1025.

23. Lei Z, Dai C, Liu X, Xiao L, Chen B. Extension of the UNIFAC model for ionic liquids. *Ind Eng Chem Res.* 2012;51(37):12135-12144.

24. Lei Z, Dai C, Wang W, Chen B. UNIFAC model for ionic liquid-CO_2 systems. *AIChE J.* 2014;60(2):716-729.

25. Song Z, Zhou T, Qi Z, Sundmacher K. Extending the UNIFAC model for ionic liquid–solute systems by combining experimental and computational databases. *AIChE J.* 2020;66(2):e16821.

26. Zhou T, Shi H, Ding X, Zhou Y. Thermodynamic modeling and rational design of ionic liquids for pre-combustion carbon capture. *Chem Eng Sci.* 2021;229:116076.

27. Stavrou M, Lampe M, Bardow A, Gross J. Continuous molecular targeting–computer-aided molecular design (CoMT–CAMD) for simultaneous process and solvent design for CO_2 capture. *Ind Eng Chem Res.* 2014;53(46):18029-18041.

28. Burger J, Papaioannou V, Gopinath S, Jackson G, Galindo A, Adjiman CS. A hierarchical method to integrated solvent and process design of physical CO_2 absorption using the SAFT-γ Mie approach. *AIChE J.* 2015;61(10):3249-3269.

29. Chong FK, Foo DCY, Eljack FT, Atilhan M, Chemmangattuvalappil NG. A systematic approach to design task-specific ionic liquids and their optimal operating conditions. *Mol Syst Des Eng.* 2016;1(1):109-121.

30. Dong K, Liu X, Dong H, Zhang X, Zhang S. Multiscale studies on ionic liquids. *Chem Rev.* 2017;117(10):6636-6695.

31. Valencia-Marquez D, Flores-Tlacuahuac A, Vasquez-Medrano R. Simultaneous optimal design of an extractive column and ionic liquid for the separation of bioethanol–water mixtures. *Ind Eng Chem Res.* 2012;51(17):5866-5880.

32. Roughton BC, Christian B, White J, Camarda KV, Gani R. Simultaneous design of ionic liquid entrainers and energy efficient azeotropic separation processes. *Comput Chem Eng.* 2012;42:248-262.

33. Chen Y, Gani R, Kontogeorgis GM, Woodley JM. Integrated ionic liquid and process design involving azeotropic separation processes. *Chem Eng Sci.* 2019;203:402-414.

34. de Riva J, Suarez-Reyes J, Moreno D, Díaz I, Ferro V, Palomar J. Ionic liquids for post-combustion CO_2 capture by physical absorption: thermodynamic, kinetic and process analysis. *Int J Greenh Gas Control.* 2017;61:61-70.

35. Mota-Martinez MT, Brandl P, Hallett JP, Mac Dowell N. Challenges and opportunities for the utilisation of ionic liquids as solvents for CO2 capture. *Mol Syst Des Eng.* 2018;3(3):560-571.

36. Palomar J, Larriba M, Lemus J, et al. Demonstrating the key role of kinetics over thermodynamics in the selection of ionic liquids for CO_2 physical absorption. *Sep Purif Technol.* 2019;213:578-586.

37. Samudra AP, Sahinidis NV. Optimization-based framework for computer-aided molecular design. *AIChE J.* 2013;59(10):3686-3701.

38. Schweidtmann AM, Huster WR, Lüthje JT, Mitsos A. Deterministic global process optimization: accurate (single-species) properties via artificial neural networks. *Comput Chem Eng.* 2019;121:67-74.

39. Huster WR, Schweidtmann AM, Lüthje JT, Mitsos A. Deterministic global superstructure-based optimization of an organic Rankine cycle. *Comput Chem Eng.* 2020;141:106996.

40. Lazzús JA. A group contribution method to predict the melting point of ionic liquids. *Fluid Phase Equilib.* 2012;313:1-6.

41. Huang Y, Dong H, Zhang X, Li C, Zhang S. A new fragment contribution-corresponding states method for physicochemical properties prediction of ionic liquids. *AIChE J.* 2013;59(4):1348-1359.

42. Paduszyński K, Domańska U. A new group contribution method for prediction of density of pure ionic liquids over a wide range of temperature and pressure. *Ind Eng Chem Res.* 2012;51(1):591-604.

43. Paduszyński K, Domańska U. Viscosity of ionic liquids: an extensive database and a new group contribution model based on a feed-forward artificial neural network. *J Chem Inf Model.* 2014;54(5):1311-1324.

44. Paulechka YU, Kabo AG, Blokhin AV, Kabo GJ, Shevelyova MP. Heat capacity of ionic liquids: experimental determination and correlations with molar volume. *J Chem Eng Data.* 2010;55(8):2719-2724.

45. Dvorak BI, Lawler DF, Fair JR, Handler NE. Evaluation of the Onda correlations for mass transfer with large random packings. *Environ Sci Technol.* 1996;30(3):945-953.

46. Mota-Martinez MT, Hallett JP, Mac Dowell N. Solvent selection and design for CO_2 capture – how we might have been missing the point. *Sustain Energy Fuels.* 2017;1(10):2078-2090.

47. Wilke CR, Chang P. Correlation of diffusion coefficients in dilute solutions. *AIChE J.* 1955;1(2):264-270.

48. Moya C, Palomar J, Gonzalez-Miquel M, Bedia J, Rodriguez F. Diffusion coefficients of CO_2 in ionic liquids estimated by gravimetry. *Ind Eng Chem Res.* 2014;53(35):13782-13789.

49. Koch-Glitsch, LP. Metal random packings. https://www.koch-glitsch.com/Technical-Documents/Brochures/Metal-Random-Packing. Accessed November 2020.

50. Song Z, Shi H, Zhang X, Zhou T. Prediction of CO_2 solubility in ionic liquids using machine learning methods. *Chem Eng Sci.* 2020;223:115752.

51. Wadekar VV. Ionic liquids as heat transfer fluids – an assessment using industrial exchanger geometries. *Appl Therm Eng.* 2017;111:1581-1587.

52. Carvalho PJ, Coutinho JAP. On the nonideality of CO_2 solutions in ionic liquids and other low volatile solvents. *J Phys Chem Lett.* 2010;1(4):774-780.

53. Couper JR, Penney WR, Fair JR, Walas SM. *Chemical Process Equipment: Selection and Design (Revised Second Edition)*. Boston: Gulf professional publishing; 2009.

54. Kılınç MR, Sahinidis NV. Exploiting integrality in the global optimization of mixed-integer nonlinear programming problems with BARON. *Optim Methods Softw.* 2018;33(3):540-562.

55. Im D, Roh K, Kim J, Eom Y, Lee JH. Economic assessment and optimization of the Selexol process with novel additives. *Int J Greenh Gas Control.* 2015;42:109-116.

56. Zhang X, Song Z, Gani R, Zhou T. Comparative economic analysis of physical, chemical, and hybrid absorption processes for carbon capture. *Ind Eng Chem Res.* 2020;59(5):2005-2012.

57. Kahrs O, Marquardt W. The validity domain of hybrid models and its application in process optimization. *Chem Eng Process.* 2007;46(11):1054-1066.

58. Schweidtmann AM, Weber JM, Wende C, Netze L, Mitsos A. Obey validity limits of data-driven models. *arXiv preprint.* 2020:arXiv:2010.03405.

59. Buxton A, Livingston AG, Pistikopoulos EN. Optimal design of solvent blends for environmental impact minimization. *AIChE J.* 1999;45(4):817-843.

Table 1. (a) Anions, cations, and cation substituent groups considered for IL design (b) Classification of cation substituent groups

(a)

Anions (G_{anion})	BF_4, Cl, DCA, NO_3, PF_6, SCN, $C(CN)_3$, HSO_4, Tf_2N, BETA, FOR, TFA, $C_3F_7CO_2$, $MeSO_4$, $EtSO_4$, $MDEGSO_4$, $MeSO_3$, TfO, NfO, TDfO, TOS, $C_{12}H_{25}PhSO_3$, methide
Cations (G_{cation})	Im13, MIm, MMIM, Py, MPyrro, MPy, MPip, NH_3, NH_2, NH, N, P
Substituents ($G_{¿}$)	CH_3, N_CH_3, P_CH_3, aN_CH_3, cycN_CH_3, CH_2, N_CH_2, P_CH_2, aN_CH_2, cycN_CH_2, CH, N_CH, OCH_2, OCH_3, CF_2, CF_3, OH

(b)

Alkyl group (G_{ag})	CH_3, N_CH_3, P_CH_3, aN_CH_3, cycN_CH_3, CH_2, N_CH_2, P_CH_2, aN_CH_2, cycN_CH_2, CH, N_CH
Non-CH_3 alkyl group (G_{nCH_3})	CH_2, N_CH_2, P_CH_2, aN_CH_2, cycN_CH_2, CH, N_CH
Functional group (G_{fg})	OCH_2, OCH_3, OH, CF_2, CF_3
Ether and hydroxyl group (G_{eh})	OCH_2, OCH_3, OH
Fluorized alkyl group (G_{fag})	CF_2, CF_3
Alkyl group linked to aromatic nitrogen (G_{aN})	aN_CH_3, aN_CH_2
Alkyl group linked to cyclic nitrogen (G_{cycN})	cycN_CH_3, cycN_CH_2
Alkyl group linked to acyclic nitrogen (G_N)	N_CH_3, N_CH_2, N_CH
Alkyl group linked to acyclic phosphorous (G_P)	P_CH_3, P_CH_2
CH_3 group directly linked to cation (G_{DCH_3})	N_CH_3, P_CH_3, aN_CH_3, cycN_CH_3
Group not directly linked to cation (G_{NDC})	CH_3, CH_2, CH, OCH_2, OCH_3, CF_2, CF_3, OH

Table 2. Input parameters for the pre-combustion carbon capture process

Input parameters for pre-combustion flue gas				
Gas composition	CO_2	0.4	Temperature (K)	313.15
	H_2	0.6	Pressure (bar)	20
Input molar flowrate (kmol/s)		10	Molar volume (L/mol)	1.28
Density (kg/m^3)		16.92	Heat capacity (kJ/kg/K)	1.72
Input parameters for the rate-based absorption process				
Inlet water temperature (K)		287	Hot steam temperature (K)	393.15
Outlet water temperature (K)		297	Steam latent heat (kJ/kg)	2201.6
Water heat capacity (kJ/kg/K)		4.18	Molar flowrate of IL (kmol/s)	3.75
Absorber temperature (K)		300	IL surface tension (N/m)	0.05
Absorber diameter (m)		5	IL association factor	0.14
Absorber thickness (m)		0.02	Packing surface area (m^2/m^3)	102
Packing diameter (m)		0.05	Packing void fraction	0.98
Flash tank thickness (m)		0.02	Packing critical surface tension (N/m)	0.075
CO_2 molar fraction in lean ILs		0.02	Flash tank diameter (m)	2.5
Isentropic coefficient		1.37	Partial molar volume of CO_2 in IL solutions (cm^3/mol)	34
Input parameters for process costing				
Capital recovery factor		0.1102	Reference cost of compressor (k$)	4714
Density of steel (kg/m^3)		7870	Reference work of compressor (kW)	22371
Cooling water price ($/ton)		0.0316	Reference cost of heat exchanger (k$)	438
Steam price ($/kg)		0.0042	Reference area of heat exchanger (m^2)	1115
Electricity price ($/kWh)		0.0775	Reference cost of pump (k$)	420.1
IL price ($/kg)		10	Reference work of pump (m^3/s)	8.2

Table 3. Computational statistics for the deterministic global optimization of the CAILPD problem

	UNIFAC-PR based models	ANN-based hybrid models
Solver	BARON	BARON
Number of discrete variables	52	52
Number of single variables	3086	439
Number of equations	3121	456
Number of nonlinear matrix entries	58032	574
Computational time	No convergence within 24 hours	5216 seconds

Table 4. Global optimization results of the studied CAILPD problem

Optimal IL group combination	2 CH_3, 2 N_CH_2, 1 OCH_2, 1 NH_2, 1 BETA
Optimal IL structure	[EEOMA][BETA] 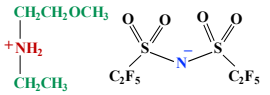 or [EMOEA][BETA] 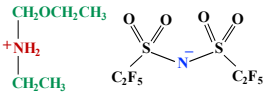
Flash tank temperature (K)	334.9
Absorber pressure (bar)	21.5
Absorber height (m)	19.4
CO_2 average solubility in the absorber	0.458
IL heat capacity in the absorber (J/g/K)	1.29
IL viscosity in the absorber (mPa·s)	10.3
CO_2 mass transfer coefficient (m/s)	1.23×10^{-4}
Gas-cooling heat exchanger area (m^2)	2090.0
IL-heating heat exchanger area (m^2)	1187.7
IL-cooling heat exchanger area (m^2)	3790.8
Cooling water consumption (ton/s)	2.17
Steam consumption (kg/s)	37.9
Compressor workload (kW)	1862.1
Pump workload (kW)	2530.3
Electricity consumption (kWh/s)	1.22
TAC (M$/year)	11.44

Figure 1. Systematic framework for computer-aided ionic liquid and rate-based absorption process design

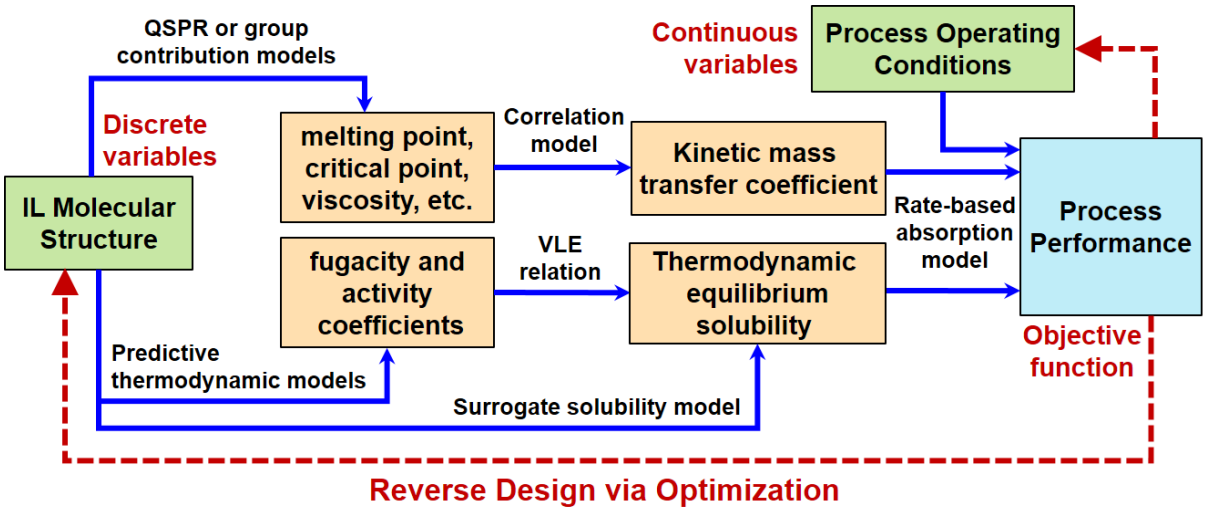

Figure 2. Representation of building groups of ionic liquids exemplified for [C_3mim][Tf_2N]

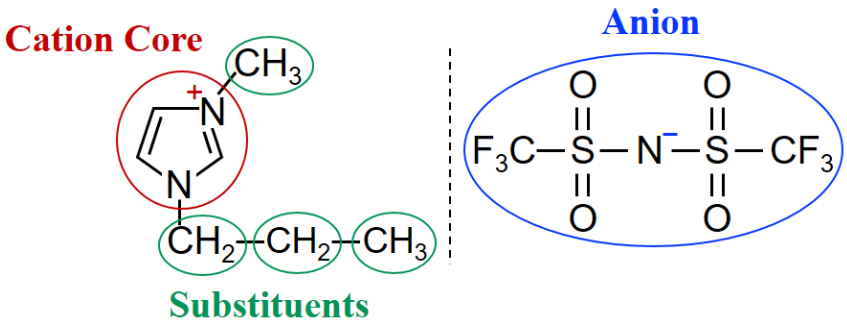

Figure 3. Models for predicting the physical and kinetic properties of ionic liquids

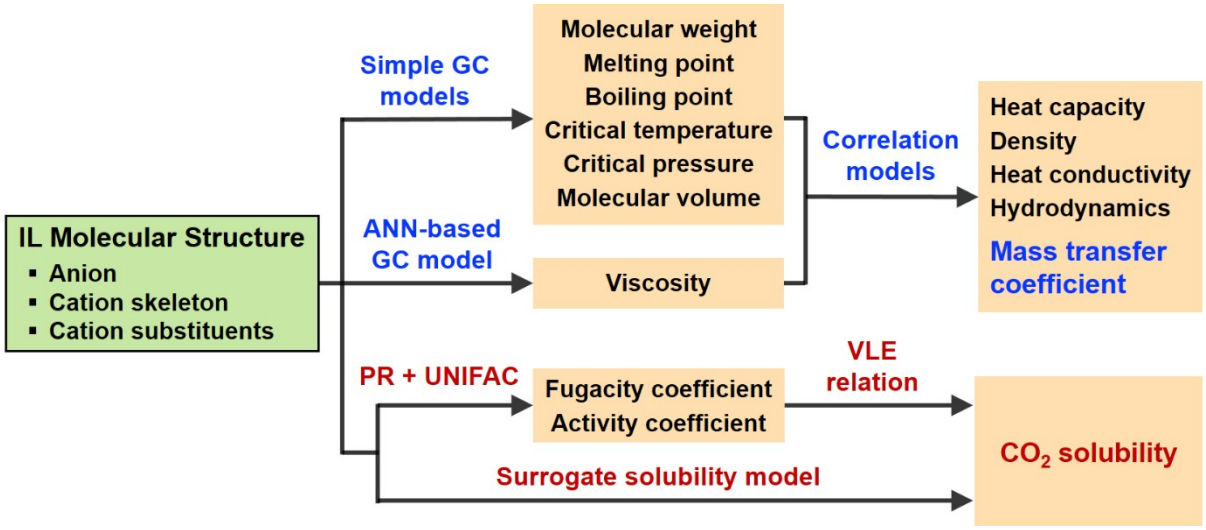

Figure 4. Schematic diagram of ionic liquid-based absorption process for carbon capture

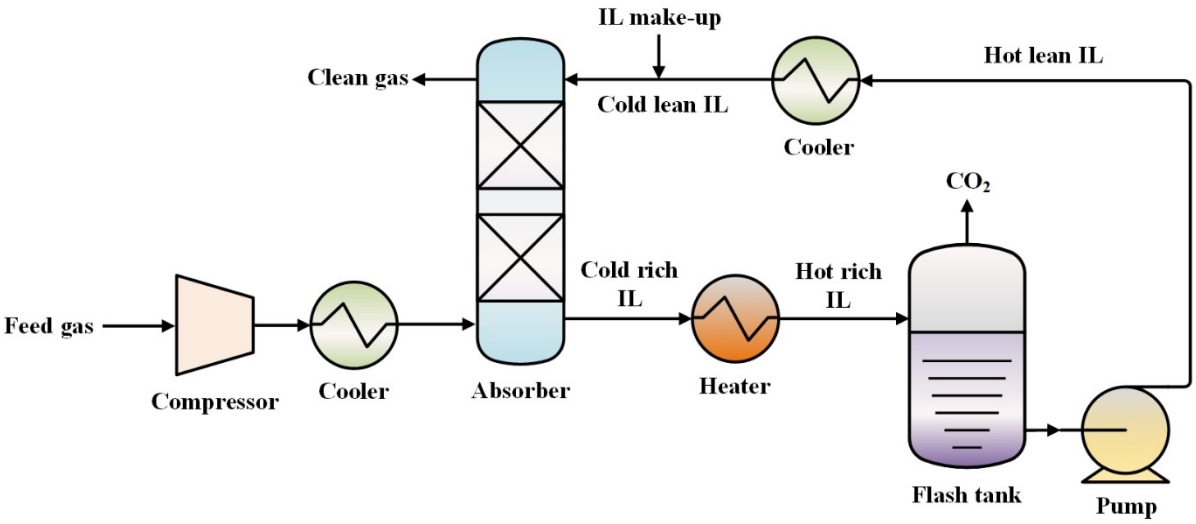

Figure 5. Cost breakdown of the optimal IL-based and DEPG-based absorption processes